FACULTAD DE CIENCIAS DEL MAR

UNIVERSIDAD DE LAS PALMAS DE GRAN CANARIA

Did the submarine volcanic eruption of El Hierro (Canary Islands) lead to a biological fertilization of the planktonic community?: evidences from *in situ* and remote sensing data in the phytoplanktonic community.

Markel Gómez Letona

Curso 2016/2017

Dr. Javier Arístegui Ruiz

Dr. Antonio Juan González Ramos

Trabajo Fin de Título para la obtención del Máster Interuniversitario en Oceanografía

Título del TFM: *Did the submarine volcanic eruption of El Hierro (Canary Islands) lead to a biological fertilization of the planktonic community?: evidences from in situ and remote sensing data in the phytoplanktonic community.*

Trabajo de fin de título presentado por Markel Gómez Letona para la obtención del título de Máster Interuniversitario en Oceanografía por la Universidad de las Palmas de Gran Canaria, la Universidad de Vigo y la Universidad de Cádiz.

El presente trabajo fue dirigido por:

Dr. Javier Arístegui Ruiz, Instituto de Oceanografía y Cambio Global (IOCAG), Universidad de Las Palmas de Gran Canaria.

Dr. Antonio Juan González Ramos, división de robótica y oceanografía computacional del Instituto Universitario de Sistemas Inteligentes y Aplicaciones Numéricas en la Ingeniería (SIANI), Universidad de Las Palmas de Gran Canaria.

Firma del estudiante | Firma de los tutores

En Las Palmas de Gran Canaria, a 27 de junio de 2017

Table of contents

Abstract

The eruption of a submarine volcano south of El Hierro (Canary Islands) in October 2011 led to major physical-chemical changes in the environment. Significant amounts of iron and inorganic nutrients were introduced to the water column from the oxidation of reduced chemical species expelled during the eruptive phase. It has been stated that the environmental fertilization with these compounds enabled the rapid restoration of the ecosystem once the volcanic activity ceased, although no biological evidence for this has been provided yet. To test the biological fertilization hypothesis on the pelagic ecosystem, we studied the evolution and variability in chlorophyll a (from *in situ* and remote sensing data) combined with information on phytoplankton and bacteria community structure (derived from Flow Cytometry) during and after the eruptive episode (from November 2011 to March 2014). Remote sensing and *in situ* data revealed that no algal bloom took place neither during nor after the eruptive episode. High satellite chl-a values registered during the eruptive phase corresponded to decoloured waters caused by sulphur compounds expelled by the volcano. *In situ* measurements of chl-a were low, in the range of the natural annual variability reported in the literature, with no significant differences between stations affected by the volcano and stations on the far field. Spatial and temporal variability in picophytoplankton (Picoeukaryotes, and *Synechococcus* and *Prochlorococcus* cyanobacteria), the most abundant size-fraction of the phytoplankton community, didn't show any response to the volcanic emissions. Only the high nucleic acid (HNA)-content bacteria (the most active groups) exhibited significantly high abundances during the most intense eruptive phase, but values were restored after the eruption ceased. Overall, our results show that the impact of the eruption on the phytoplankton community was not significant, without any evidence of biological fertilization on the pelagic ecosystem, probably due to an efficient renewal of surface waters in the region due to local currents. Temporal changes in chl-a close to the volcano area were caused by seasonal variability in the region, as well as to interannual variability associated with changes in the North Atlantic Oscillation (NAO) phases.

Key words

Submarine eruption, fertilization, picophytoplankton, bacterioplankton, chl-a, remote sensing.

Introduction

The island of El Hierro is the westernmost of the Canary Islands, which are located off the northwestern African coast (Fig. 1a). Formed 1.2 Ma ago by intraplate volcanism (Guillou et al., 1996), El Hierro is the youngest of all the islands forming the archipelago, rising from the oceanic crust at about 3500 m depth up to 1500 m above sea-level.

Historical volcanic eruptions (from the 16th century onwards) have been recorded in Lanzarote, Tenerife and La Palma islands, but not in El Hierro. After the quiescence

period following the volcanic eruption of Teneguía (La Palma Island) in 1971, in July, 2011 numerous seismic events were registered underneath El Hierro by the Instituto Geográfico Nacional (IGN), which seemed to announce an imminent volcanic episode (Carracedo et al., 2012). After more than 11,000 earthquakes, anomalous gas emissions and a vertical surface deformation of 4 cm, a submarine eruption began on October 10, 2011 in the southern submarine section of the island, 5 km off the coast at a depth of 900 m, but migrated northwards during the first three days, ceasing its advance 1.8 km off the coast, at about 300 m depth (Martí et al., 2013). On late October a first bathymetric survey was carried out, showing a 100 m-high volcanic cone at 350 m depth. A subsequent survey performed on early December reflected that the original edifice had evolved into one formed by three similarly sized cones with their top at 180-160 m depth (Carracedo et al., 2012). The activity of the eruption tended to diminish until being considered ceased by late February, 2012 (Martí et al., 2013), when the cone was situated at 88 m depth (Fraile-Nuez et al., 2012).

During the 5 month period (October, 2011 – February, 2012) in which the volcano was active, abundant eruptive materials were added to the water column, greatly altering its physical-chemical properties. These variations were not constant throughout the eruptive episode and depended on the spatial proximity to the emission zone, both horizontally and vertically. An increase in temperature and a decrease in salinity were accompanied by a discoloration of seawater associated with the emission of high-temperature hydrothermal fluids, magmatic gases and volcanic particles that reached the ocean surface and spread over a relatively vast area, being clearly visible with satellite imagery. The bubbling and degassing related to the eruption caused the input of CO_2, greatly augmenting its partial pressure (pCO_2) and the total inorganic carbon (C_T) concentration, and markedly decreasing the alkalinity (A_T) and pH levels (Fraile-Nuez et al., 2012; Santana-Casiano et al., 2013, 2016), generating changes in the carbonate chemistry, and acidification. Emission of Fe(II) and reduced species of S was also registered, which provoked a fall in the redox potential, even reaching negative values at certain depths. The oxidation of those species resulted in very low concentrations of dissolved O_2, reaching anoxic conditions in many instances in subsurface waters (Fraile-Nuez et al., 2012; Santana-Casiano et al., 2013). This compendium of environmental changes was completed with the flux of nutrients to the water column: the input of iron, whose bioavailability was increased by acidic conditions, was accompanied by increased concentrations of nitrates, phosphates and silicates in surface and, especially, subsurface waters on top of the volcanic cone (Santana-Casiano et al., 2013).

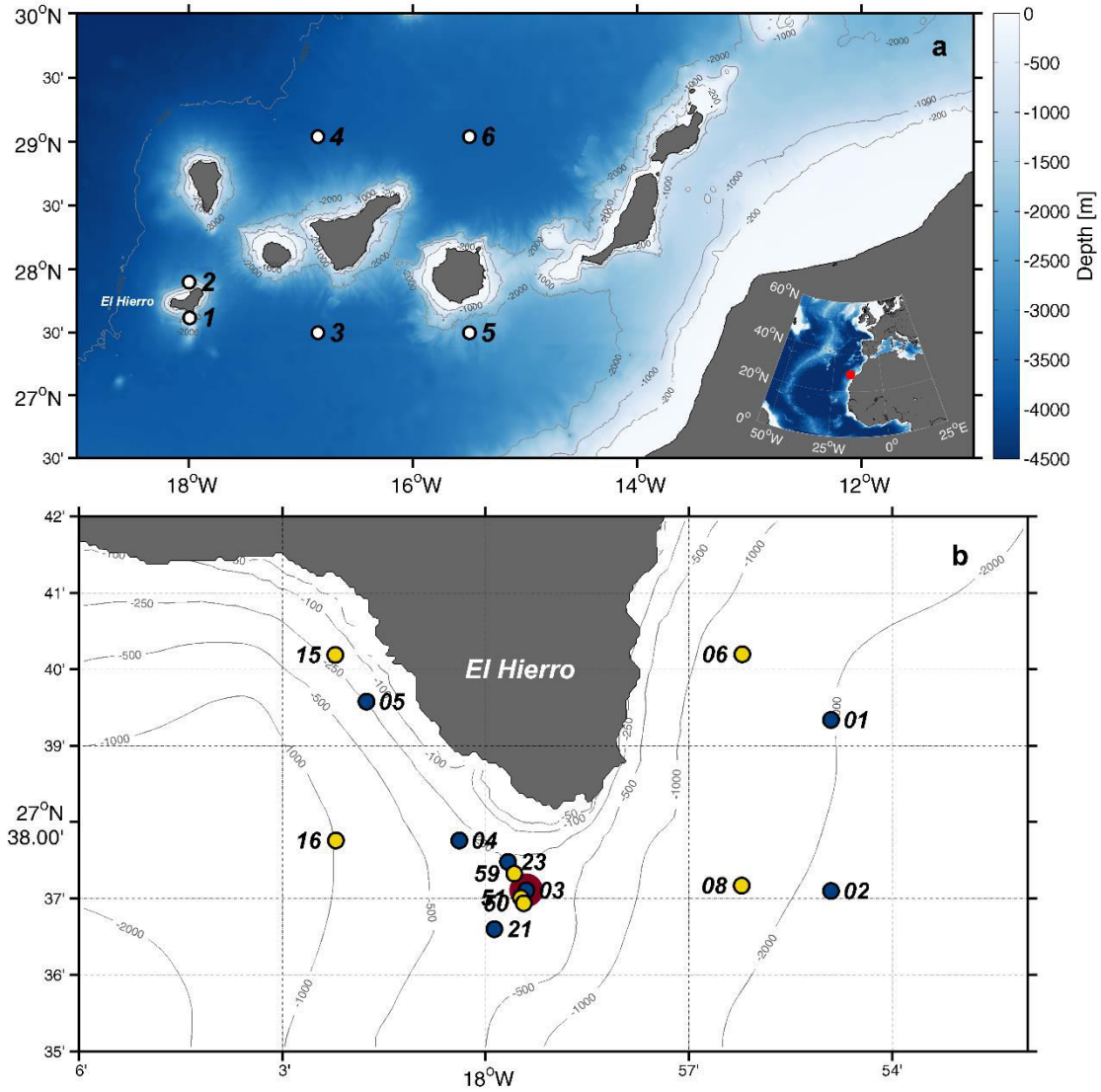

Fig. 1. a) Location of El Hierro within the Canary Islands archipelago. Dots numbered 1–6 denote areas where remote sensing chl-a has been analysed. b) Location of the stations where chl-a profiles have been derived throughout the study period. Dark blue, BBC; yellow, VUL; big, burgundy dot denotes the location of the volcano. BBC and VUL stations are paired as follows (BBC (VUL)): 01 (06); 02 (08); 03 (51); 04 (16); 05 (15); 21 (50); 23 (59).

Some of these environmental changes had a major impact on the biota. Acoustic surveys showed no presence of fish schools in the area affected by the volcano and many dead individuals were observed in the surface, due to the anoxic conditions of the surface waters (Fraile-Nuez et al., 2012). Ariza et al. (2014) studied the effect of the eruption on the Deep Scattering Layer (DSL), and observed that it altered the vertical structure of the Migrant Scattering Layers (MSL) and the patterns in the Diel Vertical Migration (DVM). The MSL was found to be strongly weaker and the upper limit of the DSL to be shallower, both anomalies being associated with an increase in surface turbidity and to dramatic decreases in dissolved O_2. Regarding phytoplanktonic organisms, very limited data has being published. Fraile-Nuez et al. (2012) reported that the response of the picoplankton depended on depth and taxa. While picophytoplankton in surface layers close to the eruption remained unaffected, at 75 m depth *Prochlorococcus* and *Synechococcus*

presented concentrations that were three and two times lower, respectively, relative to far-field measurements. On the other hand, Ferrera et al. (2015) presented an extensive work on heterotrophic bacteria. They reported that high nucleic acid (HNA)-content bacteria (the most active populations) experienced an increase in their abundance linked to the environmental changes generated by the eruption and found that bacterioplankton composition underwent minor changes, in contrast with the archaeal community, which showed no change. However, these alterations were only temporal, and the typical conditions for the microbial community were restored by January–February, 2012.

Santana-Casiano et al. (2013) suggested that the input of nutrients to the euphotic zone by the volcanic activity would act as a fertilizer, providing the ingredients for the fast recovery of the ecosystem once the eruption ceased. Nonetheless, no biological evidence has been provided supporting this hypothesis yet. In order to address this issue, we have studied the distribution of the phytoplankton community at stations affected and non-affected by the volcanic emissions, by looking at the chlorophyll concentration and picoplankton community structure, both during the eruptive and post-eruptive phases. Furthermore, *in situ* measurements have been complemented with remote sensing chlorophyll-a (chl-a) estimates in order to place in context the seasonal evolution of our measurements at a regional and inter-annual scale.

Data and Methods

Samples

The samples were collected in 10 oceanographic cruises carried out in the frame of three research projects (Bimbache (BBC), Guayota (GYT) and Vulcano (VUL)), during both the eruptive (10/2011−02/2012) and post-eruptive (from 03/2012 on) phases of the volcanic episode. The first samples were collected after 3 weeks from the onset of the eruption in BBC3 (4−9 Nov., 2011) coinciding with the strongest bubbling episode, followed by BBC5 (16−20 Nov., 2011), BBC8 (13−15 Jan., 2012), BBC10 (9−12 Feb., 2012) and BBC12 (24−26 Feb., 2012). GYT2 (17 Mar., 2012) and GYT3 (28 Apr., 2012) cruises were carried out subsequently. VUL1 (22 Mar., – 5 Apr., 2013), VUL2 (26 Oct., – 11 Nov., 2013) and VUL3 (4−24 Mar., 2014) cruises were performed further on in time.

In situ chl-a

In situ chl-a was estimated making use of a Turner Designs bench fluorometer. Water samples were collected in 0.5 L bottles, filtered using Whatman GF/F filters and preserved at -20ºC. Subsequently, chl-a was extracted employing cold acetone at 90% (v/v) for 20–24h, following Parson et al. (1984). Fluorometer measurements were performed before and after acidifying the samples with HCl, and based on them chl-a concentrations were estimated.

Fluorescence

Fluorometric measurements were carried out making use of Wet Labs ECO-AFL/FL (BBC3) and Seapoint (BBC5–12 and VUL1–3) fluorometers. Fluorescence values corresponding to Niskin bottles were paired with *in situ* chl-a measurements and linear fits were calculated ($r^2 > 0.75$). These were employed to derive chl-a profiles from fluorescence ones. In order to be able to compare BBC and VUL cruises stations were paired as shown in Fig. 1b.

Flow cytometry

Flow cytometry analyses were carried out using a BD FACSCalibur cytometer provided with an argon laser emitting at 488 nm. Picophytoplankton and bacterioplankton samples were run through the cytometer and the results were analysed employing *FlowJo* v10. Prior to the flow cytometry, bacterial samples were stained with Syto13 (Molecular Probes®) and kept in the dark for some minutes. Picophytoplankton groups were identified in bivariate scatter plots of red fluorescence (FL3) vs orange fluorescence (FL2). Similarly, bacterioplankton groups were distinguished representing green fluorescence (FL1) vs side scatter (SSC), and FL3 vs FL1. Furthermore, picocyanobacteria were identified in FL3 vs FL2 scatter plots and subsequently subtracted from high nucleic acid (HNA)-content bacteria estimates when they were overlapped. Ferrera et al. (2015) already published bacterioplankton data for BBC3–GYT3, but here the dataset is extended with three more cruises (VUL1–VUL3). Biomasses of picophytoplankton groups were estimated based on empirical relationships of carbon content per cell from biovolume measurements (MF Montero, unpublished results).

Remote sensing chl-a

Remote sensing measurements have been previously employed to monitor submarine eruptions (Coca et al., 2014; Mantas et al., 2011; Shi and Wang, 2011; Urai and Machida, 2005). In the present work, satellite-derived chl-a measurements are employed in order to synoptically follow the evolution of the phytoplanktonic community before, during and after the eruptive episode, comprising the 2010–2015 period (both years included).

Chl-a data at 1 km^2 spatial, and daily temporal resolutions was downloaded from the Copernicus Marine Environment Monitoring Service (CMEMS) website (marine.copernicus.eu). The employed product (ref. OCEANCOLOUR_ATL_CHL_L3_REP_OBSERVATIONS_009_067) has been developed by the Plymouth Marine Laboratory's (PML) Remote Sensing Group and combines Moderate-resolution Imaging Spectroradiometer (MODIS) and Visible Infrared Imaging Radiometer Suite (VIIRS) data. Chl-a time-series have been constructed for selected points in the archipelago (Fig. 1a): one above the volcano area, and five north and south of El Hierro, Tenerife and Gran Canaria islands, which are intended to represent background values for upstream/downstream conditions. However, materials expelled by the volcano, which contained abundant sulphur species, discoloured sea water and

interfered in remote sensing measurements, resulting in unrealistic chl-a concentrations (Coca et al., 2014). In order to avoid this issue, remote sensing chl-a data has been analysed using the method described in Coca et al. (2014). Briefly, they employed the downwelling diffuse attenuation coefficient at 490 nm ($K_d(490)$) to classify waters depending on their turbidity and identify areas affected by the plume:

1) Clear waters: $K_d(490) < 0.05$
2) Moderate waters: $0.13 > K_d(490) \geq 0.05$
3) Turbid waters: $K_d(490) \geq 0.13$

Both turbid and moderate waters were further divided into two subgroups based on the ratio of remote-sensing reflectance (R_{rs}) for 667 nm and 678 nm bands:

$$\frac{R_{rs}(667)}{R_{rs}(678)}$$

Considering the maximum absorption peak of chl-a at 665 nm, waters with a ratio value below 1.0 were classified as chl-a-dominated, whereas those presenting a ratio above 1.0 were regarded as not chl-a-dominated. $K_d(490)$ and R_{rs} data were downloaded from NASA's Ocean Color portal (oceancolor.gsfc.nasa.gov) at 4 km^2 spatial, and daily temporal resolutions.

Statistical analysis

Following the classification described by Ferrera et al. (2015), chl-a and flow cytometry samples have been grouped according to time of sampling, sampling site and sampling depth. Oceanographic cruises have been grouped in four distinct sampling periods: BBC3 & BBC5 (Nov., 2011), BBC8–GYT3 (Jan.–Apr., 2012), VUL1 & VUL3 (Mar., 2013 & 2014, respectively) and VUL2 (Oct.–Nov., 2013). Similarly, samples have been separated into three groups depending on which area they were collected: control, affected and volcano (see Suppl. Table 1 for details). Samples have also been classified according to their depth: subsurface (SF) waters, 0–70 m; oxygen-depleted (OD) waters, 70–200 m; deep waters (DW), >200 m.

To assess whether significant differences were present between the different groups ANOVA accompanied by *post hoc* Tukey-Kramer tests have been carried out when normalization of data was achieved. Alternatively, for data which did not follow a normal distribution Kruskal-Wallis tests supported with *post hoc* Conover tests have been performed. For all tests a significance level of 0.05 has been considered. Statistical analyses were carried out using R. Plots were also made with R using the *ggplot2* package, except maps, which were done in Matlab (*M_Map* package). CTD data analysis was done making use of the *oce* package for R.

Results

In situ chl-a estimates and profiles

Measurements of chl-a (Fig. 2) showed very low concentrations, usually between 0.05–0.3 mg·m^{-3}, rarely exceeding these values. These showed overall little, occasionally significant change between oxygen depleted (70-200 m; OD) and subsurface (0-70 m; SF) waters, although the latter consistently presented slightly higher values. The similarity was probably because the deep chlorophyll maximum (DCM) was usually located below the 70 m depth boundary. Sampling site (control/affected/volcano) turned out not to be a significant factor for the chl-a concentration at any depth. Regarding differences between phases, BBC3 & BBC5 (Nov., 2011) and VUL2 (Oct.-Nov., 2013) showed the lowest concentrations, in opposition to BBC8–GYT3 (Jan.-Apr., 2012) and VUL1 & VUL3 (Mar., 2013 & 2014). In fact, differences were significant ($p \leq 0.01$) in SF between the first two and the last two, changes being less evident in OD waters. Remarkably, there was no significant difference in chl-a values of SF waters between 2011, and 2013 and 2014 winters (BBC8–GYT3 vs VUL1 & VUL3).

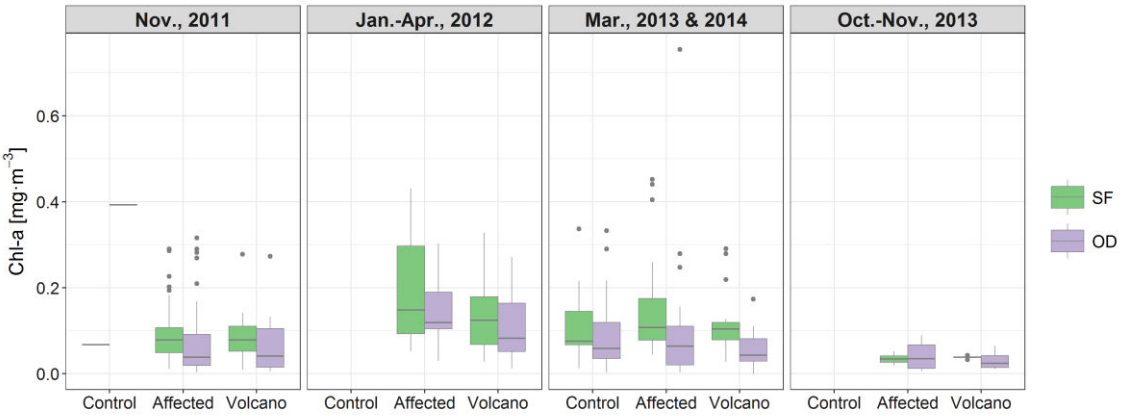

Fig. 2. *In situ* chl-a concentrations (mg·m^{-3}) grouped by sampling period, location and depth. Periods: Nov., 2011 (BBC3 & BBC5), Jan.–Apr., 2012 (BBC8–GYT3), Mar., 2013 & 2014 (VUL1 & VUL3) and Oct.–Nov., 2013 (VUL2). Locations: control (control stations), affected (any station affected by the eruption) and volcano (any station near the volcano). Depths: SF (subsurface waters, 0–70 m) and OD (oxygen-depleted waters, 70–200 m).

Chl-a profiles based on fluorometer measurements showed temporal variations of chl-a concentrations between the various cruises, differences being most evident in near surface waters. Chl-a concentrations from BBC3 (Fig. 3a) ranged between 0–0.5 mg·m^{-3}. At stations 03, 04 and 05 it roughly exceeded 0.05–0.1 mg·m^{-3} in the weak deep chlorophyll maximum (DCM). On the contrary, stations 23 and 21 showed high chl-a concentrations, with peaks reaching 0.3 and 0.5 mg·m^{-3}, respectively, the latter one being especially sharp. Unfortunately, no *in situ* measurements were carried in this station, which would have allowed to verify the estimates. Far-field stations 01 and 02 presented similar profiles, with DCMs of 0.25–35 mg·m^{-3} at 75–90 m depth. Results from BBC5 (Fig. 3b) corresponded to several repetitions of stations 03, 04 and 05. Again, low values (~0.05

mg·m^{-3}) were registered for most of the water column. DCM values only reached 0.12–0.2 mg·m^{-3} in some cases. Both in BBC3 and BBC5 two separate DCM were observed in some instances (e.g., st. 23, BBC3), the shallowest of the two being the stronger one.

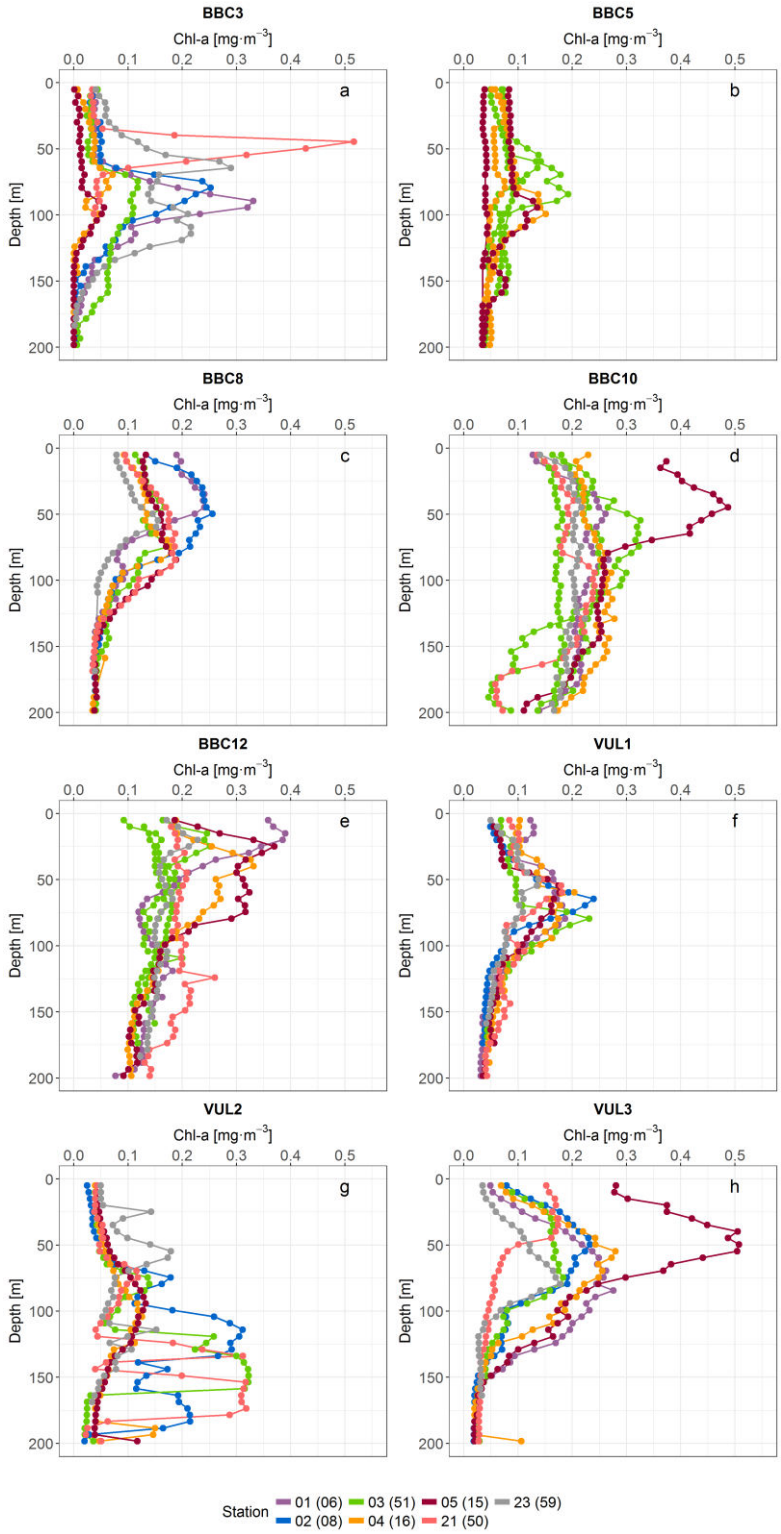

Fig. 3. Chl-a profiles derived from *in situ* chl-a data and fluorometer measurements for BBC and VUL cruises: a) BBC3 (4−9 Nov., 2011); b) BBC5 (16−20 Nov., 2011); c) BBC8 (13−15 Jan., 2012); d) BBC10 (9−12 Feb., 2012); e) BBC12 (24−26 Feb., 2012); f) VUL1 (22 Mar., – 5 Apr., 2013); g) VUL2 (26 Oct., – 11 Nov., 2013); h) VUL3 (4−24 Mar., 2014). For VUL cruises station correspondence is indicated in brackets (see Fig. 1b).

BBC8 profiles (Fig. 3c) exhibited slightly higher chl-a values in surface waters for all stations, reaching 0.1–0.2 $mg \cdot m^{-3}$, with DCMs of 0.15–0.25 $mg \cdot m^{-3}$. In BBC10 (Fig. 3d), profiles were relatively plain, and estimates ranged between 0.15–0.25 $mg \cdot m^{-3}$ for most of the water column, except in station 05, which exhibited >0.35 $mg \cdot m^{-3}$ for the first ~75 m (~0.5 $mg \cdot m^{-3}$ at the DCM). Although station 05 values seemed to be correct, for the rest of stations *in situ* and estimates derived from fluorometry disagreed, the latter being, in general, overestimated. BBC12 stations (Fig. 3e) overall presented chl-a values consistently between 0.1–0.2 $mg \cdot m^{-3}$. However, station 01 exhibited surface values of 0.35–0.4 $mg \cdot m^{-3}$, with a remarkably shallow maximum (25 m), decreasing to the aforementioned range after 50 m depth. Stations 04 and 05 showed chl-a concentrations above 0.2 $mg \cdot m^{-3}$ for the first 80 m, with a maximum of ~0.35 $mg \cdot m^{-3}$ between 25–50 m.

Regarding Vulcano cruises, in VUL1 (Fig. 3f) all chl profiles presented a similar pattern: low surface values of 0.05–0.15 $mg \cdot m^{-3}$ are followed by a DCM between 50–80 m depth, reaching 0.18–0.25 $mg \cdot m^{-3}$, and subsequently decreased to values below 0.05 $mg \cdot m^{-3}$. VUL2 (Fig. 3g) profiles showed low chl-a values (~0.05 $mg \cdot m^{-3}$), only reaching 0.12 $mg \cdot m^{-3}$ at the DCM. Finally, VUL3 profiles (Fig. 3h) exhibited a similar behaviour to those of VUL1, although the DCM was less pronounced. However, station 15 (05) stood out, as it presented surface values above 0.3 $mg \cdot m^{-3}$ and a maximum of 0.5 $mg \cdot m^{-3}$, a fact that agreed with *in situ* measurements.

Picophytoplankton and bacterioplankton abundances

Three main groups of picophytoplankton were identified in the flow cytometry analysis: picoeukaryotes, and *Synechococcus* sp. and *Prochlorococcus* sp. cyanobacteria. Their abundances showed different responses depending on the group: picoeukaryotes and *Synechococcus* followed a similar pattern, with lower abundances during BBC3 & BB5 (Nov., 2011) and VUL2 (Oct.–Nov., 2013) and higher ones during BBC8–GYT3 (Jan.–Apr., 2011) and VUL1 & VUL3 (Mar., 2013 & 2014); the opposite was true for *Prochlorococcus*.

Overall, picoeukaryotes (Fig. 4, upper panels) showed highly significant ($p<0.0001$) differences between sampling periods in SF waters. However, this was not the case when comparing BBC3 & BBC5 vs VUL2 and BBC8–GYT3 vs VUL1 & VUL3 ($p>0.01$), suggesting that changes in both cases were not clear. For OD waters similar results were obtained. As to variations between sampling sites, no significant differences were registered between them, except occasionally between stations located in the affected and volcano zones (in SF waters). Concerning sampling depth, overall SF waters showed higher abundances than OD ones, although differences were significant only sometimes. Indeed, BBC3 & BBC5 presented no significant change at all. Similarly to picoeukaryotes, *Synechococcus* (Fig. 4, lower panels) also showed significant ($p<0.0001$) differences between most sampling periods, both in SF and OD waters. However, no significant variations were registered between BBC3 & BBC5 and VUL2 in neither

depth. Similarly, no significant change was present between BBC8–GYT3 and VUL1 & VUL3 for OD waters. Regarding sampling sites, no significant differences were found when contrasting control, affected, and volcano stations. Significant changes ($p<0.01$) in the abundance of *Synechococcus* were registered between sampling depths. *Prochlorococcus* abundances (Fig. 4, central panels) presented opposed variations to the previous two groups, but these were also significant. In SF waters significance was high ($p<0.0001$) for changes between all phases; nonetheless, in OD waters no significant changes were registered between BBC3 & BBC5 and VUL2, and BBC8–GYT3 and VUL1 & VUL3. As with *Synechococcus*, no significant differences were found between sampling zones, and significant changes ($p<0.0001$) were present between sampling depths.

Fig. 4. Picophytoplankton group abundance ($\log(\text{cell}\cdot\text{mL}^{-1})$) grouped by sampling period, location and depth. From top to bottom: picoeukaryotes, *Prochlorococcus* and *Synechococcus*. Periods: Nov., 2011 (BBC3 & BBC5), Jan.–Apr., 2012 (BBC8–GYT3), Mar., 2013 & 2014 (VUL1 & VUL3) and Oct.–Nov., 2013 (VUL2). Locations: control (control stations), affected (any station affected by the eruption) and volcano (any station near the volcano). Depths: SF (subsurface waters, 0–70 m) and OD (oxygen-depleted waters, 70–200 m).

C:Chl-a ratios derived from picophytoplankton biomass and *in situ* chl-a measurements showed values that tended to range between ~50–150 in SF waters and ~15–50 in OD ones (Fig. 5). However, significant ($p<0.0001$) differences were found between each phase in SF waters, but virtually none in OD. Unlike with picophytoplankton groups there was no clear temporal pattern: ratios in SF waters decreased from BBC3 & BBC5 to

BBC8–GYT3, but surpassed all of them in VUL1 & VUL3, and further increased in VUL2, reaching values that ranged from 150 to 300. Significant differences between SF and OD waters were present during all sampling periods, except for BBC8–GYT3. Again, sampling site was not a significant factor.

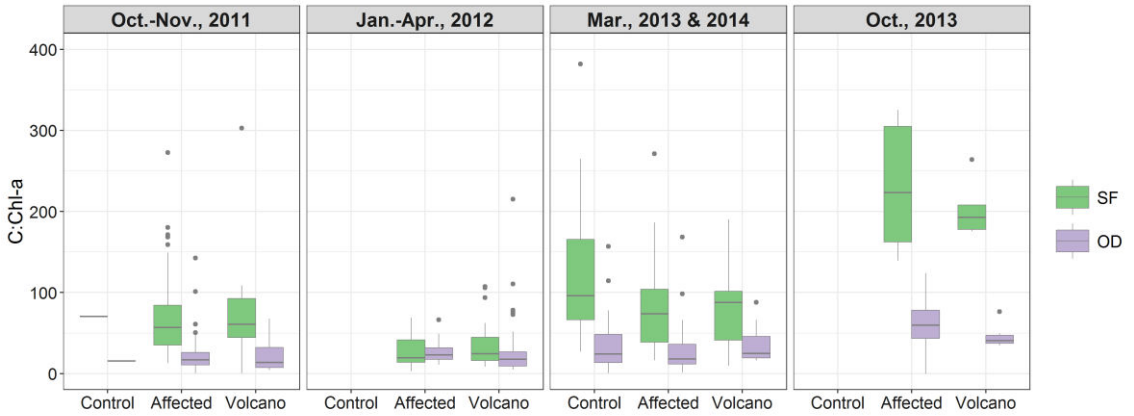

Fig. 5. C:Chl-a ratios grouped by sampling period, location and depth. Periods: Nov., 2011 (BBC3 & BBC5), Jan.–Apr., 2012 (BBC8–GYT3), Mar., 2013 & 2014 (VUL1 & VUL3) and Oct.–Nov., 2013 (VUL2). Locations: control (control stations), affected (any station affected by the eruption) and volcano (any station near the volcano). Depths: SF (subsurface waters, 0–70 m) and OD (oxygen-depleted waters, 70–200 m).

The bacterioplankton community showed distinct changes to those of picophytoplankton. During BBC3 & BBC5 (Nov. 2011), when the eruption was at its height, HNA abundances were significantly higher ($p<0.001$) in OD waters above the volcano than in the surrounding affected areas (Fig. 6, upper panels). This was also the case for DW, although differences were not significant. In contrast, SF maintained similar HNA levels in all three zones. During BBC8–GYT3 there was a significant decrease ($p<0.0001$) in HNA cell abundance in OD waters, presenting similar levels to those of affected and control stations. In DW there was still significantly higher HNA abundances in affected and, especially, volcano stations. Thereafter, a similar vertical structure was observed, cell abundances decreasing with depth, with no significant differences between sampling locations. Regarding LNA bacteria (Fig. 6, lower panels), no major changes were registered between sampling locations and periods. Most remarkably, unlike with HNA, no significant differences were found between BBC3 & BBC5 and BBC8–GYT3. However, a significant increase as registered in SF and OD waters between BBC8–GYT3 and VUL1 & VUL3. As to the relative abundance of HNA (Fig. 7), the observed general pattern was that the % of this type of bacteria increased significantly ($p<0.0001$) with depth. The HNA % observed at the volcano stations in OD during BBC3 & BBC5 (Nov. 2011) stood out as significantly high ($p < 0.01$), with values between ~75–100 %. Thus, not only did HNA bacteria increase in absolute terms during the strongest eruptive episode, but they also were more dominant. During BBC8–GYT3, the % was restored to lower values (50–75 %) and no significant changes were found between sampling areas. Similar levels were maintained during VUL1 & VUL3, but a significant drop ($p < 0.0001$) was registered in VUL2 (25–50 %).

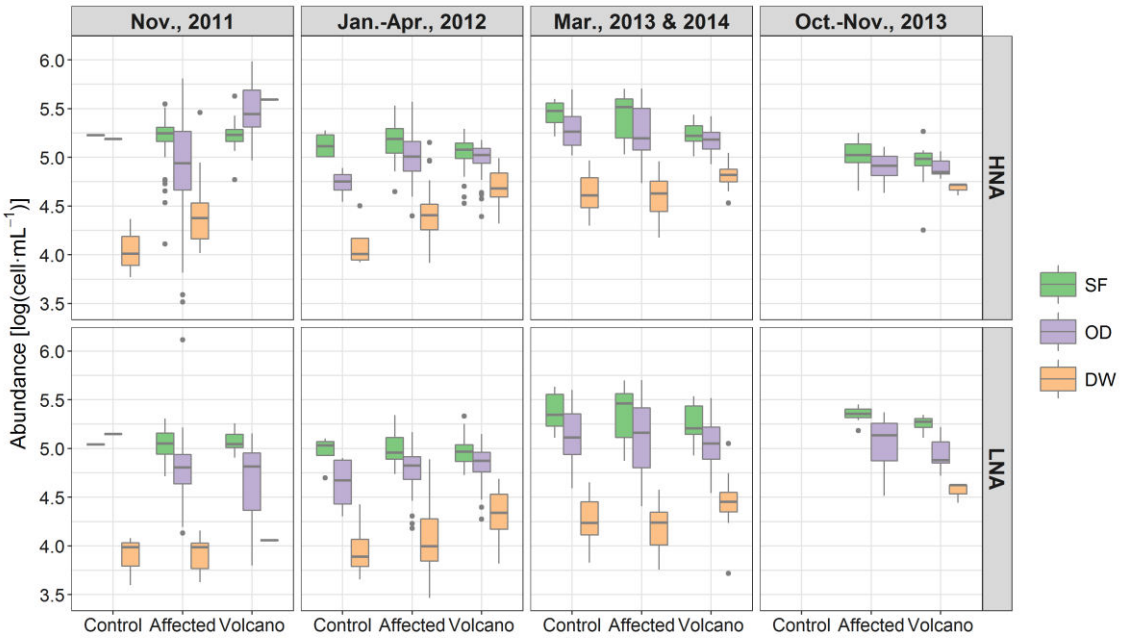

Fig. 6. Bacterioplankton group abundance (log(cell·mL^{-1})) grouped by sampling period, location and depth. From top to bottom: high nucleic acid (HNA)-content and low nucleic acid (LNA)-content bacteria. Periods: Nov., 2011 (BBC3 & BBC5), Jan.–Apr., 2012 (BBC8–GYT3), Mar., 2013 & 2014 (VUL1 & VUL3) and Oct.–Nov., 2013 (VUL2). Locations: control (control stations), affected (any station affected by the eruption) and volcano (any station near the volcano). Depths: SF (subsurface waters, 0–70 m), OD (oxygen-depleted waters, 70–200 m) and DW (deep waters, >200 m).

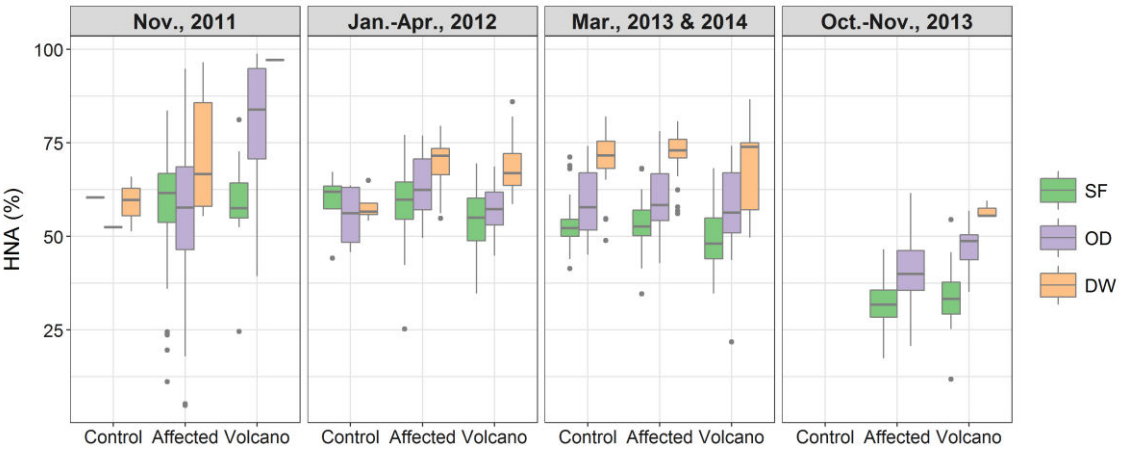

Fig. 7. High nucleic acid (HNA)-content bacteria fraction (%) grouped by sampling period, location and depth. Periods: Nov., 2011 (BBC3 & BBC5), Jan.–Apr., 2012 (BBC8–GYT3), Mar., 2013 & 2014 (VUL1 & VUL3) and Oct.–Nov., 2013 (VUL2). Locations: control (control stations), affected (any station affected by the eruption) and volcano (any station near the volcano). Depths: SF (subsurface waters, 0–70 m), OD (oxygen-depleted waters, 70–200 m) and DW (deep waters, >200 m).

Remote sensing chl-a

Remote sensing chl-a data showed a response to the eruption as soon as 13th Oct., 2011. The volcanic material emission plume was clearly distinguishable due to the reported high values of chl-a (Fig. 8a). During subsequent days and weeks the plume was consistently detected south of El Hierro, as the volcano grew and kept on expelling materials to sea water. The plume was usually seen spreading southwards and occasionally northwards (Fig. 8b), transported by the mesoscale structures that were present in the area at the time. For instance, in late Oct.-early Nov., 2011 a great plume patch was generated, and later captured by an anticyclonic eddy (Fig. 8b–d). The patch was subsequently transported southwards by the eddy, being dispersed on its way (a fact noticeable in the loss of signal strength). During this period, reported chl-a values in the plume signal usually exceeded 1–2 mg·m^{-3}, concentrations that were markedly higher than *in situ* measurements in surface waters, which never surpassed 0.1 mg·m^{-3} in BBC3 and BBC5. After nearly two months of eruption, the plume signal started weakening, although values were still visibly high over the volcano, evidencing that emissions of volcanic materials were occurring. After mid-Dec., 2011, but especially during Jan., 2012 the plume signal got weaker and was restricted to the top of the volcano (Fig. 8e), and by Feb., 2012 the plume disappeared (Fig. 8f). Results from the $K_d(490)$ and R_{rs} analysis further confirmed the fact that the reported chl-a signal of the plume was unrealistic. Waters affected by the plume were classified either as moderate, not chl-a-dominated or turbid, not chl-a-dominated waters (Fig. 9a–d). Notably, the fact that chl-a-dominated waters were correctly identified in other occasions supports this analysis. For instance, during late Feb., 2012 widespread, relatively high chl-a values of about 0.3 mg·m^{-3} were reported (Fig. 9e). The analysis classified these waters as being moderate, chl-a-dominated (Fig. 9f) and *in situ* measurements of ~0.2–0.35 mg·m^{-3} during BBC12 confirmed the correctness of remote sensing measurements

Chl-a time-series (Fig. 10) put into context the entire process. In direct relation to the aforementioned interference of the volcanic plume in the remote sensing signal, during the onset of the eruption in mid-Oct., 2011 reported chl-a values in point 1 (over the volcano) skyrocketed as a consequence of the expelled volcanic materials. Point 2 also showed some (smaller) peaks, corresponding to the spreading of the plume to the north side of El Hierro. Although several major peaks were registered in point 1 between Oct., 2011 and Feb., 2012, once the eruption ceased and the emission plume disappeared reported chl-a notably decreased, but did not go back to pre-eruptive values. Instead, chl-a concentrations during Mar., 2012 (0.17 mg·m^{-3}) were significantly higher ($p<0.0001$) than in Sep., 2011 (0.11 mg·m^{-3}). The end of the eruptive episode coincided in time with the height of the winter chl-a maximum. Indeed, 2012 presented especially high chl-a values during winter (Fig. 10), as great amounts of organic matter were transported oceanwards from the upwelling (Fig. 11c). Although this export regularly occurred during winter (Fig. 11), its magnitude varied from year to year, being influenced by the North Atlantic Oscillation (NAO) through the wind patterns: winters with high export (e.g., 2012, 2014 and 2015) were generally preceded by months of positive NAO index,

whereas low export winters (e.g., 2010 and 2011) were associated to a negative NAO index (Fig. 10).

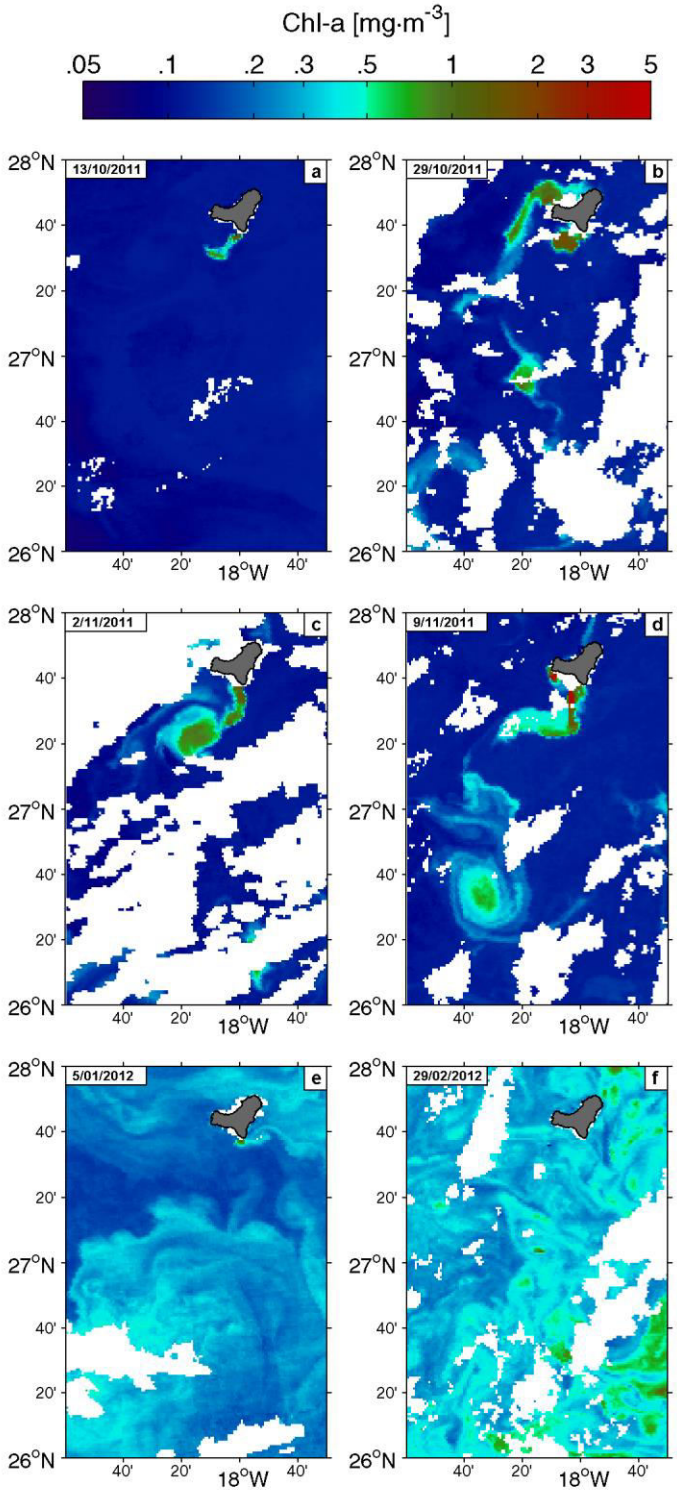

Fig. 8. Reported remote sensing chl-a (mg·m^{-3}) for selected days: a) 13/10/2011; b) 29/10/2011; c) 02/11/2011; d) 09/11/2011; e) 05/01/2012; f) 29/02/2012.

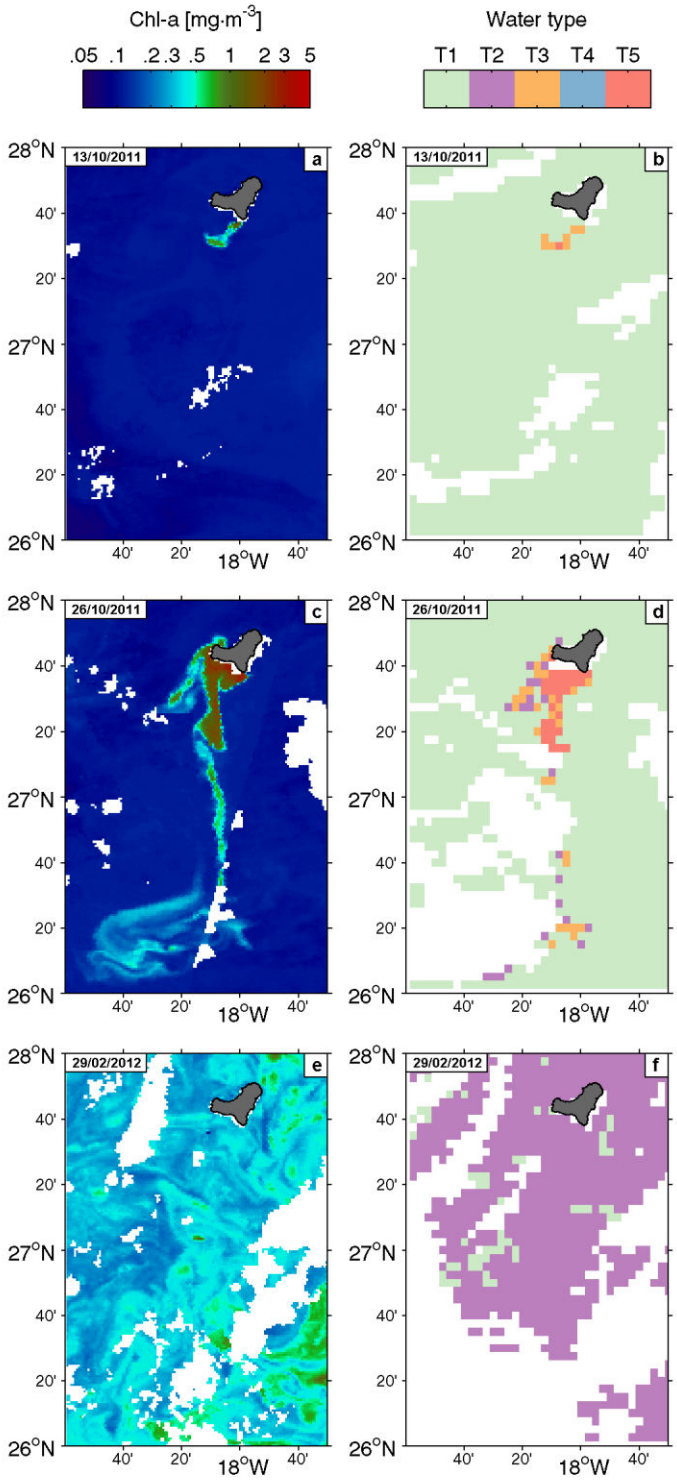

Fig. 9. Reported remote sensing chl-a (left column, mg·m^{-3}) and corresponding water classification (right column) for selected days: a) and b), 13/10/2011; c) and d), 26/10/2011; e) and f), 29/02/2012. Water classification scheme: T1: clear waters; T2: moderate, chl-a-dominated waters; T3: moderate, not chl-a-dominated waters; T4: turbid, chl-a-dominated waters; T5: turbid, not chl-a-dominated waters.

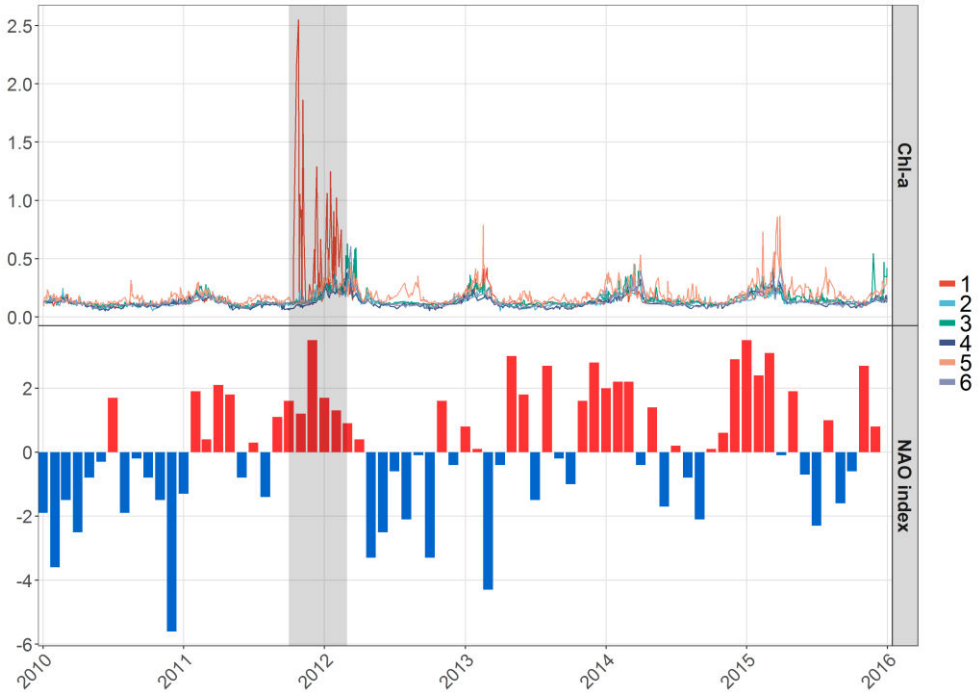

Fig. 10. Upper panel: remote sensing chl-a (mg·m^{-3}) time-series for selected points in the archipelago (Fig. 1a). Lower panel: monthly station-based North Atlantic Oscillation (NAO) index time-series. Source: NCAR (https://climatedataguide.ucar.edu/climate-data). The shaded area indicates the Oct., 2011 – Feb., 2012 time period.

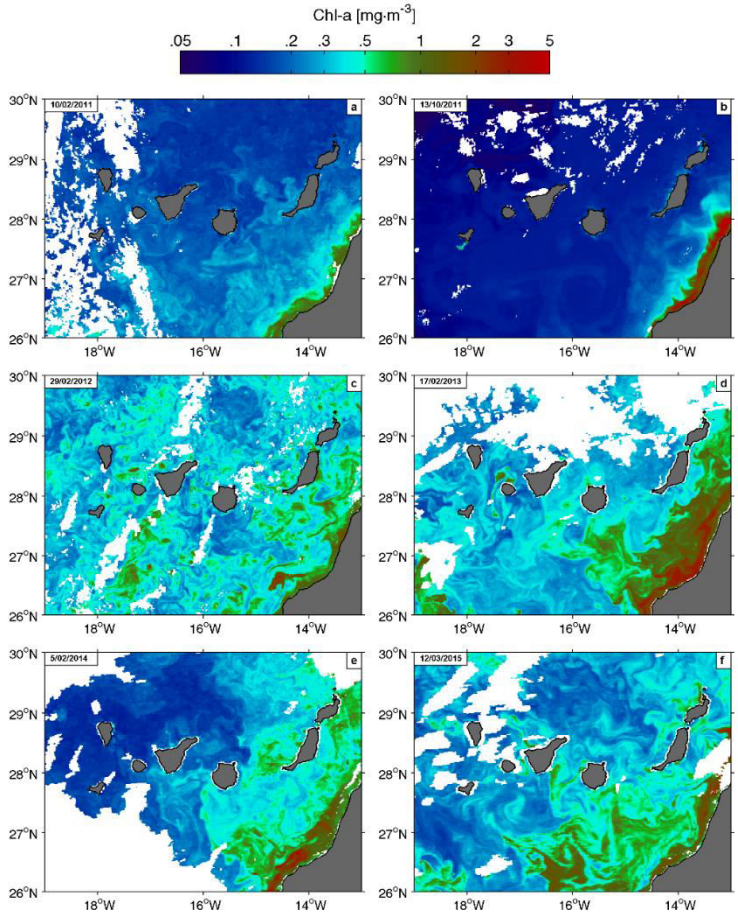

Fig. 11. Remote sensing chl-a (mg·m^{-3}) in the Canary Islands for selected days: a) 10/02/2011; b) 2011/10/13; c) 2012/02/29; d) 17/02/2013; e) 05/02/2014; f) 12/03/2015.

Discussion

The physical-chemical perturbations originated due to the submarine eruption of El Hierro –particularly related to water de-oxygenation– had a direct negative impact on epipelagic zooplankton and nekton (Ariza et al., 2014). However, no extensive work has been published assessing the effect on the phytoplankton community. Santana-Casiano et al. (2013) reported high concentrations of Fe(II), phosphates, nitrates and silica in the water column above the volcano, with maximum values located at ~100 m depth during Nov., 2011. Subsurface concentrations decreased with time, reaching minimum values in Feb., 2012, whereas augments were registered in surface waters. Based on this evidence, the authors affirmed that the same eruption that caused a damaging effect on the marine biota produced a fertilization, providing the necessary nutrients to rapidly restore the ecosystem. Nonetheless, no biological evidence supporting this hypothesis has been published yet.

Changes in chl-a

Although a considerable amount of literature exists on how the ash emitted by subaerial volcanos could trigger the proliferation of algal organisms, very little has been written on the potential effect of submarine eruptions. The work of Mantas et al. (2011) is one of the very few on this matter. They studied the Home Reef eruption (Tonga, Southwestern Pacific Ocean) in 2006 using various types of remote sensing data (including MODIS chl-a data), and they registered a phytoplankton bloom presenting chl-a concentrations an order of magnitude higher than background values. The bloom coincided spatially and temporally with a plume of discoloured water associated with the volcano, the plume preceding the bloom by 9 days. Based on the comparison of R_{rs} values between the Home Reef bloom and a previous confirmed *Trichodesmium* sp. bloom in the northeastern Australian coast, they concluded that the Home Reef bloom was also dominated by cyanobacteria from that same genus. The authors attributed the bloom to the enrichment of the waters by Fe which, at acid pH levels, would be bioavailable as Fe(II).

The remote sensing data analysis carried out in the present work was done aiming to search for any similar phenomena. Although multiple patches of abnormally high chl-a were initially observed (mainly between Oct.–Nov., 2011, when the most intense eruptive episodes occurred), these were not associated with algal blooms; rather, they were erroneous estimates consequence of the interference produced by discoloured waters, as previously reported by Coca et al. (2014). The plume, formed by expelled volcanic materials, contained great amounts of sulphur compounds (Fraile-Nuez et al., 2012; Santana-Casiano et al., 2013), producing a signal that interfered with that of chl-a, which resulted in unrealistic estimates by the remote sensing chl-a algorithms. This was confirmed by *in situ* chl-a measurements: surface values of <0.1 mg·m^{-3} contrast with remote sensing estimates of over 1–2 mg·m^{-3}. *In situ* estimates were supported by the results from the water classification scheme proposed by Coca et al. (2014), as plume waters were classified as not chl-a-dominated (either moderate or turbid). Although the analytical procedure seemed to operate adequately (it also correctly identified chl-a-

dominated waters) caution is required when the R_{rs} ratio values fall near the 1.0 boundary. This limit stablished by Coca et al. (2014) was selected on empirical grounds and therefore not considered to be infallible. Hence, occasionally some areas classified as not chl-a-dominated are registered in the upwelling area (not shown), possibly influenced by sediment resuspension in shallow waters. Similarly, some pixels classified as chl-a-dominated can be observed in the edges of volcanic plumes (Fig. 9d). These could be correctly classified and be consequence of the mitigation of the adverse conditions within the plume or simply be an error of the classification scheme due to the dispersion of the plume and the subsequent change in the spectral properties of the waters, making them fall below 1.0. In either case, this type of pixel represents only a small portion of the plumes where they occur.

The effect of the volcanic plume in the chl-a time-series was clearly visible. Multiple peaks of extremely high chl-a concentrations were reported south of El Hierro and occasionally north (Fig. 10, points 1 and 2, respectively), between Oct., 2011 and Feb., 2012. Again, these values were unrealistic and did not indicate the flourishment of any algal bloom. However, after the eruptive episode (the plume signal vanished by Feb., 2012), chl-a values were not restored to pre-eruptive levels. Although the difference between pre- and post-eruptive chl-a concentrations (0.11 vs 0.17 $mg \cdot m^{-3}$, respectively) might not seem great, considering the oligotrophic nature of El Hierro's waters it supposed a considerable change and, indeed, turned out to be significant. However, the increase was not related to the volcano, but it was rather due to the coincidence with the late winter chl-a maximum, as the primary producers were favoured by the ascent of nutrient from deep waters, consequence of the vertical mixing originated due to the cooling of surface waters. Besides, the export of chl-a from the upwelling (Fig. 11) can have an impact in the whole Canary Islands region, although the effect tends to decrease westwards. The intensity of the export varied from year to year and appeared to be positively correlated with the NAO index. Upwelling favourable winds have been described to also be positively correlated to the NAO index (Arístegui et al., 2004; Cropper et al., 2014) and thus they are deemed a potential link that could explain the relation.

In situ chl-a measurements in the first 70 m depth also showed significant differences between the beginning eruptive phase (Nov., 2011) and the end of it (Jan.–Apr., 2012), with higher concentrations in the latter. However, chl-a was still low, barely reaching 0.2 $mg \cdot m^{-3}$, values which lie within previous reported concentrations for El Hierro (Arístegui, 1990). These values were not significantly different from those registered in late winter 2013 and 2014. Besides, measurements from Oct.-Nov., 2013 resulted in slightly lower values than for the same period of time in 2011, when the eruption was at its height, implying that chl-a was not altered. Moreover, sampling location proved not to be a significant factor for chl-a. Hence, the eruption yielded no significant impact on chl-a concentrations, whose variations are attributable to the seasonal cycle. The limited effect of the volcano might be partially explained by the efficient renewal of affected waters by the southward flow, as it has been observed by remote sensing data (Fig. 8).

Chl-a profiles showed a similar temporal evolution, surface values increasing from BBC3 to BBC12. The vertical distribution followed the typical pattern, increasing chl-a concentration with depth, reaching a DCM at ~50-75 m due to photoacclimation. Profiles were far less pronounced during winter months (e.g., BBC10 and BBC12) as a consequence of vertical mixing and subsequent increase of chl-a in surface waters. Nonetheless, some profiles exhibited distinct behaviours. During BBC3, station 21 (southwest, close to the volcano) presented a very sharp DCM. In 10 m (35–45 m) chl-a values increased an order of magnitude, from 0.05 to 0.5 $mg \cdot m^{-3}$, nearly doubling values from control stations 01 and 02. At 70 m depth low values were restored. Nearby stations did not show analogous peaks: station 03 (above the volcano), presented a relatively plain profile and station 23 (north, close to the volcano) exhibited a DCM that was similar to those of control stations. An incorrect measurement by the fluorometer, consequence of the influence of volcanic materials, might explain observed values, although no similar potential failures were observed in other stations. *In situ* chl-a measurements would have proven to be decisive but, unfortunately, none were performed in station 21 and thus no definite answer can be given. Apart from BBC3-st.03, station 05 (15) showed high chl-a concentrations that stood out above the rest of the stations on two separate occasions. During BBC10 and VUL3, values in the first ~75 m of the water column were higher than in the rest of stations. However, considering that the cruises were carried out in winter months (Feb., 2012 and Mar., 2013, respectively) the registered values (0.3–0.5 $mg \cdot m^{-3}$), which agreed with *in situ* measurements, were not anomalously high. For instance, Arístegui et al. (1997) reported chl-a concentrations of 0.16–0.77 $mg \cdot m^{-3}$ at 25 m depth south of Gran Canaria during late winter. Arístegui et al. (2001) found chl-a concentrations above 1 $mg \cdot m^{-3}$ in surface waters and Schmoker et al. (2012) values above 0.8 $mg \cdot m^{-3}$ at 20–70 m depth, both during winter blooms in coastal waters of the same island. The difference between stations might be due to station 05 (15) being the shallowest one (< 250 m, Fig. 1b). As such, the vertical mixing and subsequent input of nutrients to the euphotic zone would be more effective and could result in higher chl-a concentrations consequence of increased biological activity of phytoplankton.

Effect on picophytoplankton and bacterioplankton communities

Marine enviroments with poor nutrient concentrations and low values of chl-a (such as the ones observed in El Hierro) tend to be dominanted by small phytoplanktonic organisms. Indeed, picophytoplankton and, especially, *Prochlorococcus* sp. have been observed to be the dominant photoautotrophic organisms in the oligotrophic waters of the eastern subtropical North Atlantic, although *Synechococcus* sp. and picoeukaryotes also contribute considerably (Morán et al., 2004; Zubkov et al., 2000). Results from the flow cytometry analysis show cell abundances of the same order of those reported by Zubkov et al. (2000) for 25–30ºN (~21ºW), with *Prochlorococcus* sp. > *Synechococcus* sp. > picoeukaryotes. However, abundances within each group significantly differed depending on the sampling period.

Prochlorococcus sp. showed higher values during cruises carried out in autumn, when waters tend to be still warm and stratified after the annual temperature maxima in Aug.–

Sep., whereas during winter, when waters are cool and well mixed, abundances were lower; the opposite was true for *Synechococcus* sp. and picoeukaryotes. These changes agree with the distributions observed by Zubkov et al. (2000, 1998), who reported *Prochlorococcus* sp. to be more dominant in warm, oligotrophic waters, and *Synechococcus* sp. and picoeukaryotes in cooler, mesotrophic ones. Changes were significant between most of the cruises in subsurface waters for all three groups, but far less evident below 70 m depth, where seasonal environmental changes are milder. Moreover, the fact that overall no significant changes were found between control, affected and volcano stations suggests a limited impact on picoplankton group abundances by the eruption.

Autotrophic C:Chl-a ratios of picoplankton showed significant changes between sampling periods mainly in subsurface waters. Nevertheless, unlike picoplankton group abundances, C:Chl-a ratios did not follow any clear seasonal pattern. Vázquez-Domínguez et al. (2013) described a seasonal cycle of picoplankton C:Chl-a ratios in the Cantabrian sea with maximum values during summer (~100), when high temperature and irradiance, and low inorganic nutrients were present, and minimum values during winter (~20), along with the lowest temperature and irradiance, and high inorganic nutrients. Similar results were obtained by Jakobsen and Markager (2016) for coastal waters in Denmark, with summer and winter values of 20–96 and 7.7–33, respectively (with no size distinction). However, C:Chl-a ratios also vary between phytoplankton groups: lower ratios are usually observed in microphytoplankton, whereas higher values are typical of picophytoplankton. Anabalón et al. (2014) reported winter values of 30–104 for the microplankton fraction and 168–175 for the picoplankton in the first 150 m of the water column in Cape Ghir. Sathyendranath et al. (2009) reported values of 15-107 for diatoms and 123–147 for *Prochlorococcus* sp. based on data of multiple locations. Another source of variability is the pigment composition of the species: *Synechococcus* sp. is known to present chl-a as their principal pigment, with phycobiliproteins as accessory ones (Waterbury et al., 1979); on the other hand, *Prochlorococcus* sp. present divinyl derivates of chl-a and -b, along with zeaxastin and α-carotene (Goericke and Repeta, 1992). Finally, depth also importantly conditions C:Chl-a ratios, as cells increment their chl-a content to compensate the reduction of irradiance and be able to meet their energetic demands. This reduces C:Chl-a values in deep waters, as seen in Fig. 5. C:Chl-a ratios observed in the present work agree reasonably well with those found in literature. Higher than normal values during Oct., 2013 were due to high *Prochlorococcus* sp. biomass (Suppl. Fig. 1) and very low chl-a concentrations. Similarly, high C:Chl-a ratios for Mar., 2013 and 2014 were result of increased picoplankton biomass. Considering that sampling location was not a significant factor determining C:Chl-a ratio distributions these results could be atributable to natural variabiliy.

The anaylsis of bacterioplankton aimed to extend already published data on this matter (Ferrera et al., 2015). While LNA showed little to virtually no change between sampling areas and period, HNA abundaces were altered. Sinficantly high abundaces were registered below 70 m depth over the volcano during Nov., 2011, when the eruptive

activity was most intense. Likewise, increased HNA % indicates that these type of bacteria, considered to be more active, were more dominant during the eruptive period, altough with no significant differences between sampling locations. The observed increase in HNA bacteria seems to be related to the volcano, possibly due to the presence of high concentrations of nutrients. However, it had a short-lived impact, as usual values were restored once the eruptive activity started to cease.

Conclusions

Remote sensing and *in situ* data revealed that no algal bloom was registered neither during nor after the eruptive episode. Reported unrealistically high values of satellite chl-a were due to the failure of algorithms in plume waters that were decoloured by expelled volcanic materials (which included sulphur compounds). *In situ* measurements of chl-a corroborated this, as typical values for the region were found both during and after the eruption. Besides, temporal changes were presumably controlled by seasonal variations of environmental factors that control biological activity (such as stratification of waters). Picoplanktonic groups followed a similar pattern, with *Prochlorococcus* sp. being more abundant during warmer months, and *Synechococcus* sp. and picoeukaryotes during cooler ones, although always within usual values. C:Chl-a ratios did not show any clear pattern, but agreed with values for picoplankton found in the literature. Interestingly, the sampling location was not a significant factor that explained the distribution of any of the biological variables, further suggesting the limited effect of the eruption. HNA bacteria were positively affected by the eruption, especially in relatively deep waters above the volcano. However, the effect was limited to the period when the eruption was most intense and values were restored as soon as it started to cease. In sum, the effect of the eruption on the pelagic phytoplankton community was not significant, as changes were dominated by seasonal variability rather than by the physical-chemical alterations produced by the volcano. The limited effect might partially be explained by the efficient renewal of waters in the zone. Thus, the assertion that the input of nutrients by the volcano provided the grounds for a fast recovery of the ecosystem lacks support.

Acknowledgements

We thank Eugenio Fraile (Instituto Español de Oceanografía) for inviting us to participate in the BBC and VUL cruises, and to the ULPGC for funding the GYT cruises. The Group of Biological Oceanography (GOB) of the ULPGC contributed to the collection and analyses of *in situ* data along the different cruises. JM Coca (ULPGC) advised on the analyses of remote sensing data.

References

Anabalón, V., Arístegui, J., Morales, C.E., Andrade, I., Benavides, M., Correa-Ramírez, M.A., Espino, M., Ettahiri, O., Hormazabal, S., Makaoui, A., Montero, M.F., Orbi, A., 2014. The

structure of planktonic communities under variable coastal upwelling conditions off Cape Ghir (31ºN) in the Canary Current System (NW Africa). Prog. Oceanogr. 120, 320–339. doi:10.1016/j.pocean.2013.10.015

Arístegui, J., 1990. La distribución de la clorofila a en aguas de Canarias. Boletín del Inst. Español Oceanogr. 6, 61–72.

Arístegui, J., Álvarez-Salgado, X.A., Barton, E.D., Figueiras, F.G., Hernández-León, S., Roy, C., Santos, A.M.P., 2004. Oceanography and fisheries of the Canary current/Iberian region of the eastern North Atlantic (18a,E), in: Robinson, A.R., Brink, K.H. (Eds.), The Sea. Harvard University Press, Harvard, MA, pp. 877–932.

Arístegui, J., Hernández-león, S., Montero, M.F., Gómez, M. a Y., 2001. The seasonal planktonic cycle in coastal waters of the Canary Islands. Sci. Mar. 65, 51–58. doi:10.3989/scimar.2001.65s151

Arístegui, J., Tett, P., Hernández-Guerra, A., Basterretxea, G., Montero, M.F., Wild, K., Sangrá, P., Hernández-León, S., Cantón, M., García-Braun, J.A., Pacheco, M., Barton, E.D., 1997. The influence of island-generated eddies on chlorophyll distribution: A study of mesoscale variation around Gran Canaria. Deep. Res. Part I Oceanogr. Res. Pap. 44, 71–96. doi:10.1016/S0967-0637(96)00093-3

Ariza, A., Kaartvedt, S., Røstad, A., Garijo, J.C., Arístegui, J., Fraile-Nuez, E., Hernández-León, S., 2014. The submarine volcano eruption off El Hierro Island: Effects on the scattering migrant biota and the evolution of the pelagic communities. PLoS One 9. doi:10.1371/journal.pone.0102354

Carracedo, C.J., Pérez Torrado, F., Rodríguez González, A., Soler, V., Fernández Turiel, J.L., Troll, V.R., Wiesmaier, S., 2012. The 2011 submarine volcanic eruption in El Hierro (Canary Islands). Geol. Today 28, 53–58. doi:10.1038/443502a

Coca, J., Ohde, T., Redondo, A., García-Weil, L., Santana-Casiano, M., González-Dávila, M., Arístegui, J., Nuez, E.F., Ramos, A.G., 2014. Remote sensing of the El Hierro submarine volcanic eruption plume. Int. J. Remote Sens. 35, 6573–6598. doi:10.1080/01431161.2014.960613

Cropper, T.E., Hanna, E., Bigg, G.R., 2014. Spatial and temporal seasonal trends in coastal upwelling off Northwest Africa, 1981-2012. Deep. Res. Part I Oceanogr. Res. Pap. 86, 94–111. doi:10.1016/j.dsr.2014.01.007

Ferrera, I., Arístegui, J., González, J.M., Montero, M.F., Fraile-Nuez, E., Gasol, J.M., 2015. Transient changes in bacterioplankton communities induced by the submarine volcanic eruption of El Hierro (Canary Islands). PLoS One 10, 1–17. doi:10.1371/journal.pone.0118136

Fraile-Nuez, E., González-Dávila, M., Santana-Casiano, J.M., Arístegui, J., Alonso-González, I.J., Hernández-León, S., Blanco, M.J., Rodríguez-Santana, A., Hernández-Guerra, A., Gelado-Caballero, M.D., Eugenio, F., Marcello, J., de Armas, D., Domínguez-Yanes, J.F., Montero, M.F., Laetsch, D.R., Vélez-Belchí, P., Ramos, A., Ariza, A. V., Comas-Rodríguez, I., Benítez-Barrios, V.M., 2012. The submarine volcano eruption at the island of El Hierro: physical-chemical perturbation and biological response. Sci. Rep. 2, 1–7. doi:10.1038/srep00486

Goericke, R., Repeta, D.J., 1992. The pigments of Prochlorococcus marinus: The presence of divinylchlorophyll a and b in a marine procaryote. Limnol. Oceanogr. 37, 425–433. doi:10.4319/lo.1992.37.2.0425

Guillou, H., Carracedo, J.C., Pérez Torrado, F., Rodriguez Badiola, E., 1996. K-Ar ages and magnetic stratigraphy of a hotspot-induced, fast grown oceanic island: El Hierro, Canary Islands. J. Volcanol. Geotherm. Res. 73, 141–155. doi:10.1016/0377-0273(96)00021-2

Jakobsen, H.H., Markager, S., 2016. Carbon-to-chlorophyll ratio for phytoplankton in temperate coastal waters: Seasonal patterns and relationship to nutrients. Limnol. Oceanogr. 61, 1853–1868. doi:10.1002/lno.10338

Mantas, V.M., Pereira, A.J.S.C., Morais, P. V., 2011. Plumes of discolored water of volcanic origin and possible implications for algal communities. The case of the Home Reef eruption of 2006 (Tonga, Southwest Pacific Ocean). Remote Sens. Environ. 115, 1341–1352. doi:10.1016/j.rse.2011.01.014

Martí, J., Pinel, V., López, C., Geyer, A., Abella, R., Tárraga, M., Blanco, M.J., Castro, A., Rodríguez, C., 2013. Causes and mechanisms of the 2011-2012 El Hierro (Canary Islands) submarine eruption. J. Geophys. Res. Solid Earth 118, 823–839. doi:10.1002/jgrb.50087

Morán, X.A.G., Fernández, E., Pérez, V., 2004. Size-fractionated primary production, bacterial production and net community production in subtropical and tropical domains of the oligotrophic NE Atlantic in autumn. Mar. Ecol. Prog. Ser. 274, 17–29. doi:10.3354/meps274017

Parson, T.R., Maita, Y., Lalli, C.M., 1984. A Manual of Chemical and Biological Methods for Seawater Analysis, A Manual of Chemical and Biological Methods for Seawater Analysis. doi:10.1016/B978-0-08-030287-4.50002-5

Santana-Casiano, J.M., Fraile-Nuez, E., González-Dávila, M., Baker, E.T., Resing, J.A., Walker, S.L., 2016. Significant discharge of CO2 from hydrothermalism associated with the submarine volcano of El Hierro Island. Sci. Reports 6, 25686. doi:10.1038/srep25686

Santana-Casiano, J.M., González-Dávila, M., Fraile-Nuez, E., de Armas, D., González, A.G., Domínguez-Yanes, J.F., Escánez, J., 2013. The natural ocean acidification and fertilization event caused by the submarine eruption of El Hierro. Sci. Rep. 3, 1140. doi:10.1038/srep01140

Sathyendranath, S., Stuart, V., Nair, A., Oka, K., Nakane, T., Bouman, H., Forget, M.H., Maass, H., Platt, T., 2009. Carbon-to-chlorophyll ratio and growth rate of phytoplankton in the sea. Mar. Ecol. Prog. Ser. 383, 73–84. doi:10.3354/meps07998

Schmoker, C., Arístegui, J., Hernández-León, S., 2012. Planktonic biomass variability during a late winter bloom in the subtropical waters off the Canary Islands. J. Mar. Syst. 95, 24–31. doi:10.1016/j.jmarsys.2012.01.008

Shi, W., Wang, M., 2011. Satellite Observations of Environmental Changes from the Tonga Volcano Eruption in the Southern Tropical Pacific. Int. J. Remote Sens. 32, 5785–5796. doi:10.1080/01431161.2010.507679

Urai, M., Machida, S., 2005. Discolored seawater detection using ASTER reflectance products: A case study of Satsuma-Iwojima, Japan. Remote Sens. Environ. 99, 95–104. doi:10.1016/j.rse.2005.04.028

Vázquez-Domínguez, E., Morán, X.A.G., López-Urrutia, A., 2013. Photoacclimation of picophytoplankton in the central Cantabrian Sea. Mar. Ecol. Prog. Ser. 493, 43–56. doi:10.3354/meps10549

Waterbury, J.B., Watson, S.W., Guillard, R.R.L., Brand, L.E., 1979. Widespread occurrence of a unicellular, marine, planktonic cyanobacterium. Nature 277, 293–294. doi:10.1038/277293a0

Zubkov, M. V., Sleigh, M.A., Burkill, P.H., Leakey, R.J.G., 2000. Picoplankton community structure on the Atlantic Meridional Transect: A comparison between seasons. Prog. Oceanogr. 45, 369–386. doi:10.1016/S0079-6611(00)00008-2

Zubkov, M. V., Sleigh, M.A., Tarran, G.A., Burkill, P.H., Leakey, R.J.G., 1998. Picoplanktonic community structure on an Atlantic transect from 50ºN to 50ºS. Deep. Res. Part I Oceanogr. Res. Pap. 45, 1339–1355. doi:10.1016/S0967-0637(98)00015-6

Supplementary material

Suppl. Fig. 1. Picoplankton group biomass (mg C·m^{-3}) grouped by sampling period, location and depth. From top to bottom: picoeukaryotes, Prochlorococcus and Synechococcus. Periods: Nov., 2011 (BBC3 & BBC5), Jan.–Apr., 2012 (BBC8–GYT3), Mar., 2013 & 2014 (VUL1 & VUL3) and Oct.–Nov., 2013 (VUL2). Locations: control (control stations), affected (any station affected by the eruption) and volcano (any station near the volcano). Depths: SF (subsurface waters, 0–70 m) and OD (oxygen-depleted waters, 70–200 m).

Suppl. Table 1. Metadata of samples for *in situ* chl-a and flow cytometry analyses. 4 digit stations correspond to those repeated over several cruises; station code (9SSR) means: 9, "repetition"; SS, station number; and R, number of the repetition. For instance, "9014" would be the 4th repetition of station 01. * depths or cruises in which no samples for *in situ* chl-a measurements were collected.

Cruise	Station	Longitude	Latitude	Depths [m]						Location
BBC3 (4−9 Nov., 2011)	01	-17.914833	27.655	5	25*	75				Control
	03	-17.993	27.618	5*						Volcano
	04	-18.006333	27.6291667	25	50	75	150	266*		Volcano
	05	-18.029	27.6588333	5	25	75	100	125		Affected
	06	-18.066667	27.6551667	5	25	75				Affected
	08	-18.216	27.7305	5	25	50	75			Affected
	10	-18.1405	27.655	25	50	62*	150			Affected
	11	-18.140333	27.621	5	25	63	76	150		Affected
	12	-18.066667	27.5811667	5	25	50	70	150		Affected
	14	-17.990167	27.544	5	25	50	75	150		Affected
	15	-17.988667	27.581	5	25*	50	64	150		Affected
	17	-18.0625	27.5431667	5	25	50	70	150*		Affected
	18	-18.2145	27.655	5	25	50	83	105		Affected
	20	-18.141167	27.5461667	5	25	50	78	167		Affected
	22	-17.989167	27.6253333	20*	75*	90*				Volcano
	23	-17.9945	27.6246667	10	75	90	190*			Volcano
	24	-18.0075	27.6293333	5	25	50	75			Volcano
	9014	-18.486833	27.057	5	25	50	75	150		Affected
BBC5 (16−20 Nov., 2011)	9032	-17.995167	27.618	5	25	50	75	160*		Volcano
	9034	-17.995167	27.6178333	5	25	50	75	100	125	Volcano
	9043	-18.006167	27.6295	5	25	50	75	125		Volcano
	9044	-18.006333	27.6283333	5	25	50				Volcano

	9053	-18.03	27.6591667	5	25	50	75	125		Affected
	9054	-18.031	27.6593333	5	25	50	75	100	125	Affected
	01	-18.185	27.7595	5	25	50	75	150		Affected
	02	-18.223333	27.7786667	5	25	58	75	100		Affected
	03	-18.203667	27.8201667	5	25	50	75	100		Affected
	05	-18.109167	27.773	5	25	55	75	100		Affected
	06	-18.125667	27.7986667	5	25	50	75	100		Affected
	07	-18.164667	27.8228333	5	25	50	88	105		Affected
	08	-18.117167	27.8243333	5	25	50	80	100		Affected
	09	-18.092	27.7986667	5	25	50	75	100		Affected
	10	-18.062667	27.7886667	5	25	50	75	100		Affected
	11	-18.0395	27.7791667	5	25	50	75	100		Affected
	12	-18.043833	27.8208333	5	25	50	75	100		Affected
	13	-18.077333	27.8271667	5	25	50	75	100		Affected
	14	-18.096333	27.853	5	25	50	75	100		Affected
	15	-18.039333	27.8823333	5	25	50	75	100		Affected
	16	-18.034667	27.8511667	5	25	50	75	100		Affected
	17	-18.012333	27.8263333	5	25	50	75	100		Affected
	18	-17.9845	27.8498333	5	25	50	75	100		Affected
	19	-17.991167	27.8776667	5	25	50	73	100		Affected
BBC8 (13−15 Jan., 2012) *	01	-17.895	27.7695	5	44	50	75	100		Affected
	02	-17.914833	27.7341667	5	25	75	100	150		Affected
	03	-17.957833	27.656	5	50	75	100	150		Affected
	04	-17.956667	27.6191667	5	50	75	100	150		Affected
	05	-17.958667	27.683	5	50	75	100	150	200	Affected
	06	-17.917167	27.6803333	5	50	75	100	150		Affected

	07	-17.917667	27.7073333	5	50	85	100	150				Affected
	08	-17.947167	27.7058333	5	50	75	100	150				Affected
	09	-17.881167	27.7485	5	50	75	100	150				Affected
	9013	-17.915	27.6556667	5	50	75	100	150				Control
	9022	-17.9145	27.6183333	5	25	75	100	150				Affected
	9036	-17.989167	27.6183333	5	25	50	100					Volcano
	9046	-18.005667	27.6285	5	50	75	86	150				Volcano
	9056	-18.028167	27.659	5	50	75	100	150				Affected
	9213	-17.997333	27.6105	25	50	75	100	150				Volcano
	9233	-17.994667	27.6246667	5	57	75	100	150				Volcano
BBC10 (9−12 Feb., 2012)	01	-18.0675	27.6843333	5	25	50	75	100	150	200*	400*	Affected
	02	-18.066667	27.6576667	5	50	150	200*					Affected
	03	-18.066667	27.6293333	5*	25*	50	75*	100*	150*	200*		Affected
	04	-18.0675	27.612	5	50	150	200*					Affected
	05	-18.064333	27.5908333	5	50	150	200*					Affected
	06	-18.027833	27.6283333	5	50	165	200*					Affected
	07	-18.0265	27.6096667	5	25*	100	200					Affected
	08	-18.025667	27.5851667	5	56	150	200					Affected
	9215	-17.9965	27.6111667	5*	25*	50*	75*	100*	150*			Affected
	9038	-17.9955	27.6186667	5	25	50	100	125				Volcano
	9039	-17.9955	27.62	5	25	50	100	160				Volcano
	9047	-18.0055	27.6283333	5	50	100	150	200*				Volcano
	9057	-18.028833	27.6578333	5	25	50	100	150				Affected
	9234	-17.995167	27.625	5	25	50	100	215				Volcano
BBC12 (24−26 Feb., 2012) *	01	-18.0265	27.6281667	5	50	100	200	300	400			Affected
	03	-17.997833	27.5876667	5	50	100	200					Affected

	04	-18.0265	27.5851667	5	50	100	200						Affected
	06	-18.002833	27.62	5	50	100	200	300	423				Affected
	9015	-17.9135	27.6571667	5	75	125							Control
	90310	-17.992667	27.6198333	5	20	30	50	70	86				Volcano
	90311	-17.993833	27.6213333	5	25	50	75	100	165				Volcano
	90312	-17.995	27.62	5	25	50	75	100	185				Volcano
	9048	-18.005333	27.6286667	5	25	40	100	200	300				Volcano
	9216	-17.997833	27.6101667	5	50	100	200	300	400				Volcano
GYT2 (17 Mar., 2012)	04	-18.00567	27.6285	5	25	60	100	125	250				Volcano
	23	-17.99467	27.62467	5	35	50*	75	100	125				Volcano
GYT3 (28 Apr., 2012)	10			5	50	75	100	200	300				Volcano
	21	-17.99733	27.6105	5	50	75	100	200	300				Volcano
	23	-17.99467	27.62467	5	50	75	100	150	180				Volcano
	V	27.61833	-17.98917	2	25*	50	75	100	115*				Volcano
VUL1 (22 Mar., – 5 Apr., 2013)	02	-17.837	27.7695	5	50	75	100	150	200*	400*	600*	800*	1000*	Control
	04	-17.906333	27.7328333	5	50	75	100	150	200*	400*	600*	800*	1000*	Control
	06	-17.936833	27.67	5	50	75	100	150	200*	400*	600*	800*	1000*	Control
	07	-17.886667	27.687	5	50	60	100	150	200*	400*	600*	800*	1000*	Control
	08	-17.937	27.6195	5	50	75	100	150	200*	400*	600*	800*	1000*	Control
	11	-17.987	27.4698333	5	50	75	100	150	200*	400*	600*	800*	1000*	Affected
	13	-17.987167	27.5698333	5	50	60	100	150	200*	400*	600*	800*	1000*	Affected
	16	-18.036833	27.6198333	5	50	75	100	150	200*	400*	600*	800*	1000*	Affected
	21	-18.1025	27.6546667	5	50	75	100	150	200*	400*	600*	800*	1000*	Affected
	23	-18.136833	27.6848333	5	50	75	100	150	200*	400*	600*	800*	1000*	Affected
	25	-18.204667	27.7175	5	50	75	100	150	200*	400*	600*	800*	1000*	Affected
	27	-18.18	27.7645	5	50	75	100	150	200*	400*	600*			Affected

	50	-17.990667	27.6156667	5*	50*	75*	100*	150*	200*	315*	323*	326*	Volcano
	51	-17.991333	27.6168333	5*	50*	75*	100*	150*	239*	246*	250*		Volcano
	52	-17.992	27.6176667	5*	50*	75*	100*	150*	197*	205*	209*		Volcano
	53	-17.992	27.6185	5*	50*	85*	100*	150*	176*	183*			Volcano
	54	-17.992667	27.6188333	5*	50*	75*	100*	148*	153*	162*			Volcano
	55	-17.993	27.6193333	5*	50*	75*	109*	113*					Volcano
	56	-17.993333	27.6203333	50	75*	82*	91*						Volcano
	57	-17.994	27.6203333	5*	50*	75*	100*	115*	123*				Volcano
	58	-17.993167	27.6216667	50	75*	100*	150*	170*	177*				Volcano
	59	-17.993	27.6221667	5*	50*	75*	100*	158*	163*				Volcano
	13	-17.987	27.57	5*	25*	50*	75*	100*	150*				Affected
	15	-18.036833	27.6696667	5*	25*	50*	75*	100*	150*				Affected
	16	-18.0365	27.6198333	5*	25*	50*	75*	100*	150*				Affected
	19	-18.086833	27.6196667	5*	25*	50*	75*	100*	150*				Affected
	20	-18.087	27.6805	5	25	50	75	100	150				Affected
	21	-18.1025	27.6546667	5	25	50*	75	100	150				Affected
	22	-18.137	27.6481667	5	25	50	75	100	150				Affected
VUL2 (26 Oct., – 11 Nov., 2013)	23	-18.136833	27.685	5	25	50	75	100	150				Affected
	50	-17.990667	27.6156667	5*	25*	50*	75*	100*	150*	334*			Volcano
	51	-17.991333	27.6168333	5*	25*	50*	75*	100*	150*	246*			Volcano
	52	-17.992	27.6176667	5	25	50	75	100	150	204*			Volcano
	53	-17.992	27.6185	5*	25*	50*	75*	100*	150*				Volcano
	55	-17.993	27.6193333	5*	25*	50*	75*	100*	150*				Volcano
	56	-17.993333	27.6203333	5*	25*	50*	75*	150*					Volcano
	58	-17.993167	27.6216667	5	25	50*	75	100	150	176*			Volcano
VUL3 (4−24 Mar., 2014)	02	-17.837	27.7695	5	25	50	75	100	150				Control

	07	-17.886667	27.687	25*	65*	75*	150*				Control
	08	-17.937167	27.6195	5	25	50	75	100	150	400	Control
	13	-17.987167	27.5698333	5	25	50	75	100	150		Affected
	15	-18.037	27.6698333	5	25	50	75	100	150		Affected
	16	-18.036833	27.6198333	5*	25*	50*	75*	100*	150*		Affected
	17	-18.036833	27.57	5	25	50	75	100	150	250	Affected
	18	-18.0595	27.6433333	50*	68*	100*	150*				Affected
	19	-18.087167	27.6198333	5	25	50	75	100	150		Affected
	20	-18.087	27.6803333	5	25	50	75	100	150*		Affected
	21	-18.1025	27.6546667	5	25	50	75*	100	150		Affected
	22	-18.137	27.648	5	25	50*	75	100*	150*		Affected
	23	-18.136833	27.6848333	5*	25*	50*	75*	100*	150*		Affected
	50	-17.990667	27.6156667	5	25	50	75	100	150	250*	Volcano
	51	-17.991333	27.6168333	5*	25*	50*	75*	100*	150*	247*	Volcano
	52	-17.992	27.6176667	5	25	50	75	100	150	205*	Volcano
	53	-17.992	27.6185	5*	25*	50*	75*	100*	150*		Volcano
	54	-17.992667	27.6188333	5*	25*	50*	75*	100*	150*		Volcano
	55	-17.993	27.6193333	5	25	75	100	132*			Volcano
	56	-17.993333	27.6203333	5*	25*	50*	75*	92*			Volcano
	58	-17.993167	27.6216667	5*	25	50	75	100	150		Volcano
	61	-17.993167	27.6195	5	25	50	75	100	117		Volcano

Descripción detallada de las actividades desarrolladas durante la realización del TFT

Las actividades realizadas durante el TFM se han centrado en el análisis de diferentes tipos de datos, tanto *in situ* (proporcionados por el grupo de investigación que hizo las medidas) como de teledetección (descargados de los portales de diferentes organizaciones), para determinar el impacto de la erupción submarina de El Hierro sobre la comunidad fitoplanctónica.

El análisis de datos *in situ* ha constado de tres partes:

- Medidas de chl-a.
- Medidas de fluorescencia. En combinación con las medidas in situ de chl-a se han generado regresiones lineales que a la postre se han empleado para generar perfiles verticales de chl-a.
- Medidas de citometría de flujo. Se han empleado para identificar la presencia de ciertos organismos planctónicos (picofitoplancton y bacterias), así como para estimar su abundancia. Además se han calculado las biomasas de cada grupo basándose en relaciones empíricas, y posteriormente se han estimado los ratios de Carbono:Chl-a.

El análisis de datos de teledetección ha consistido en:

- Evolución temporal y espacial de la chl-a.
- Los datos de reflectancia y el coeficiente de atenuación difusa de *downwelling* se han empleado para determinar la naturaleza de los píxeles de chl-a mencionados en el punto anterior. Se han clasificado en función de su turbidez y se ha deducido si dichos píxeles estaban dominados por chl-a o no.

Asimismo, se han comparado los resultados de chl-a *in situ* y de teledetección, con objetivo de observar si existían diferencias o no.

El análisis de los datos se ha completado con la aplicación de test estadísticos.

A lo largo de la realización del TFM se ha llevado a cabo una lectura de bibliografía relacionada con la materia de estudio.

Formación recibida

Durante la realización del TFM se me ha enseñado a analizar datos de citometría de flujo con el software *Flowjo*, permitiéndome identificar y estimar la abundancia de organismos fitoplanctónicos y bacterias.

Por otro lado, he podido emplear datos de teledetección más allá de las usuales variables como temperatura, clorofila, etc. Concretamente, la utilización de datos como los de reflectancia en bandas concretas del espectro visible me ha proporcionado una visión más amplia de las opciones que otorgan las medidas de teledetección.

Nivel de integración e implicación dentro del departamento y relaciones con el personal

Estimo que he llegado a tener una alta integración e implicación dentro del grupo de investigación en el que he desarrollado el TFM. El hecho de haber realizado el Trabajo de Fin de Grado con el mismo grupo de investigación el curso previo ha supuesto una enorme ventaja, ya que ha posibilitado un fácil entendimiento entre las partes y ha hecho que el desarrollo del trabajo se haya dado de forma fluida.

Aspectos positivos y negativos más significativos relacionados con el desarrollo del TFT

Me ha resultado muy gratificante poder estudiar el efecto que tuvo la erupción de El Hierro sobre la comunidad fitoplanctónica. La ocasión de estudiar los efectos de una erupción submarina se da muy pocas veces, por lo que valoro mucho que se me brindara esta oportunidad.

De forma más general, uno de los principales aspecto positivos es la fluidez con la que he podido desarrollar el trabajo. Como he mencionado en el apartado anterior, la culpa de ello la tiene en gran medida el hecho de haber continuado con el mismo grupo de investigación con el que realicé el TFG. Ello ha posibilitado la buena comunicación y entendimiento desde el primer día, hecho que sin duda ha contribuido de forma importante que pudiese realizar una buena labor.

No destacaría ningún aspecto negativo relevante.

Valoración personal del aprendizaje conseguido a lo largo del TFT

Considero que, en general, el aprendizaje adquirido durante el desarrollo del TFM podría serme útil en un futuro, ya que he profundizado mi conocimiento sobre diversos temas. Asimismo, creo que puedo afirmar que, comparando con el TFG, he madurado en el sentido académico. Creo que la labor que he realizado está más pulida con respecto al curso previo, tanto en cuanto a planificación y desarrollo como en cuanto a la redacción del trabajo propiamente dicho. Por ello considero que he avanzado y me muestro satisfecho.